Original Study **Open Access**

Czesław Machelski*, Piotr Tomala

Shell Deformation During the Construction of Record Span Soil-steel Buried Structure in Ras-Al-Khaimah (UAE)

https://doi.org/10.2478/sgem-2023-0007
received March 18, 2022; accepted April 3, 2023.

Abstract: The algorithm presented in this paper concerns the processing of data in the form of coordinates of measurement points located around the structure periphery, obtained from the geodetic measurements. The geometric parameter used here to study the deformation of the steel shell is the change of curvature. It is used to estimate the bending moment and hence the normal stress in the corrugated steel shell. The results given in the examples of calculations of the analyzed structure show the possibility of determining places with extreme values. For this purpose, a dense layout of measuring points and use the precision geodesy technique is necessary. Of significant importance in stress estimation is the correction of the geodetic measurement base. This is due to the fact that the points in the initial measurement do not lie on a section of the circle as a reference curve, used to determine the deformation of the shell.

Keywords: Soil-steel structure; geodetic measurements; strain-gauge measurement; deformations; internal forces

1 Introduction

The buried bridges are considered competitive structures being a cost-effective alternative to concrete bridges with similar span sizes. This frequently stimulates designers to push their limits and expand the different areas of application including its performance. This also implies that most design methods are continuously being developed to address new market challenges and at the same time, to seek for better design and construction. Despite being in existence for several decades, soil-steel bridges are usually designed by using simple analytical methods. Their rapid development and reaching ever larger spans require the use of more and more advanced computational tools, often with the use of FEM. Advanced computational techniques allow designers to calculate structures with asymmetric backfill, especially taking into account linearly variable backfills [23] (so-called sloping terrain). Such topography is common in mountainous areas.

Large-span structures are more sensitive to asymmetric backfilling, which is why undesirable deformations may occur faster. So far, structures with record spans have been subjected to detailed monitoring with the use of electro-resistant strain gauges which, by measuring strains, have provided information on the level of stresses. On the basis of stresses, the level of utility of the structure was set and, at the same time, the structure's status was set as safe or not.

Strain gauge measurements, however, are quite expensive and make it possible to calculate internal forces only at measuring points. Measuring techniques using optical fibers provide a continuous picture of changes in internal forces, but they are still too expensive. Both the aforementioned measurement techniques require the involvement of scientific units or research institutes in the research project because only such units have specialized personnel and advanced dedicated equipment with software. The method described in this paper allows for estimating safety on the basis of simple geodetic measurements. It is fast, does not require any specialized equipment, and gives results consistent with those obtained on the basis of strain gauge measurements.

2 Subject of research

The structure presented and analyzed in this paper was built in 2020 in Ras Al Khaimah in the United Arab Emirates. For now, it seems to be the largest (in a term of

***Corresponding author: Piotr Tomala,** ViaCon Polska Sp. z o.o Rydzyna, E-mail: piotr.tomala.1972@gmail.com
Czesław Machelski, Wroclaw University of Science and Technology

Figure 1: Grade separation during construction – general view.

span) corrugated steel buried bridge in the world [5]. The geometrical parameters of the structure are as follows: span L = 32.64 m, rise H = 9.57 m, and crown radius R = 29.68 m, corrugation type UltraCor 500 × 237 × 12 mm.

This paper presents the results of monitoring of buried structure during its construction stage. Geodetic techniques and strain gauge measurements were used to monitor the shell deformations [1]. For the analysis of the changes in the steel shell, the radius of curvature was taken. This allows for estimating the bending effects around the periphery of the shell. This can be achieved when comparing the shape of the structure after assembly to its initial form. The algorithm of the analysis presented in this paper is based on the changes of the coordinates of measurement points.

The simplest and very effective form of monitoring which is applicable for buried soil-steel bridges is the geodetic total station survey as shown on Fig. 1. This type of monitoring is sufficiently accurate due to the expected quite big structure deformations. Here, we are talking about changes in geometry for both, construction and operation stages..

When tracking the position of measurement points located around the structure's periphery, we can analyze the change of its geometry. Determined in this way, the form of deformation can be successfully used for the estimation of internal forces [1, 4].

In the case of individual structures and sometimes during live load tests, the strain gauge measurements are also used. They are commonly used for direct estimation of internal forces. They can be also used to calculate the form of deformation using the numerical algorithms discussed in [1, 3, 4, 8, 9].

Such measurements can be successfully used to determine the contact interactions [1, 9, 10, 11], that is, the forces between the steel shell and the surrounding soil as shown on Fig.2.

Direct pressure measurement is performed with the use of soil pressure gauges [12]. Therefore, depending on the function of the soil-steel structure as well as the geometrical parameters (e.g extremely large spans), various monitoring techniques are used. In this paper, the transformed results of geodetic measurements will be compared with obtained strain gauge measurements.

3 Process of deformations during the structure construction stage

In order to maintain assumed in the design process structure geometry, it is essential to control the backfilling process.[1]. It is especially important for flexible structures made of corrugated steel plates when the spans are reaching the limits. Predicting the shell deformation based on the numerical analyses is difficult because the results are extremely sensitive to the backfilling procedure and also seasonal breaks [1, 13].

Fig.2presents the example of a regular double-hinged arch structure with radius R founded on rigid footings. Results of the analysis presented in this paper are concerned with the construction stage where z_g represents the level of backfilling as shown on Fig.2. The stage when the surrounded soil was placed to the level of z_g was analyzed. It was also assumed that the geometry is symmetrical. The interaction of soil is represented by contact forces: normal $p(\varphi)$ and tangential $t(\varphi)$.

Steel shell deformation that occurred during the construction process of the bridge can be described by two characteristic deflections shown in Fig.2 There is upward deflection of the crown point (w) called *peaking* and horizontal *narrowing* of the haunch points ($2u$).

The proportions between the deflections of $w$and $2u$in the process of placement of the surrounding soil are changed [1, 4, 14, 15]. Both components of displacement of the measurement points in this paper are presented as radial displacement r.

Fig. 3 shows the layout of measurement points around the structure periphery, which is used for geodetic surveys. Table 1 presents the results of measurements of the structure crown point displacements at characteristic stages of construction, depending on the backfill level z_g. The differences in the backfill thickness included in the last line relate to the intended, asymmetrical deformation of the coating, which is shown in Fig. 4. Asymmetrical placement of the backfill layers is used in the case of twin structures [13], and the soil interactions are not symmetrical [44]. From the results presented in Table

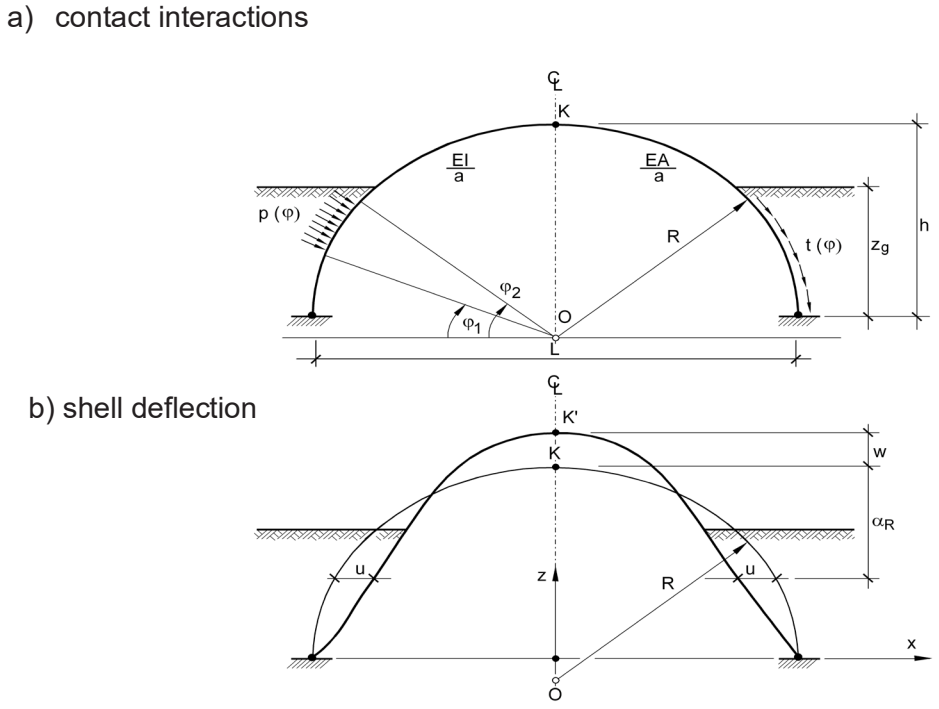

Figure 2: Scheme of shell deflections and contact forces.

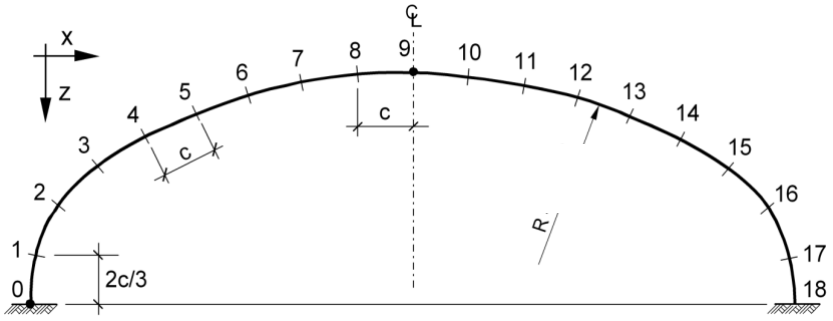

Figure 3: Scheme of examined structure.

Table 1: Components of displacements of points No.9 and 11.

Construction Stage		A	B	C	D	E	F
w (mm)	9	34.7	92.3	28.8	–46.8	–89.4	–116.3
	11	19.6	–7.9	–55.2	–116.9	–143.2	–164.7
u (mm)	9	–4.5	15.3	4.3	5.1	3.3	3.2
	11	2.1	33.5	23.9	29.2	26.7	25.7
z_g(m)		7.54/7.25	9.78/9.99	10.44/11.04	10.48/11.32	11.07/11.92	11.73/12.32
Date		25.09	01.11	08.12	15.12	31.12	15.01

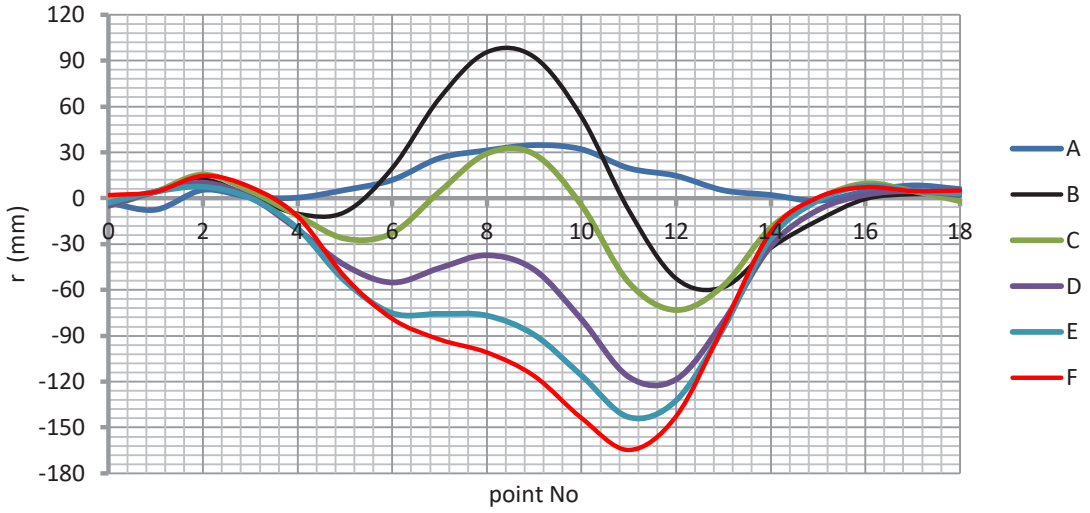

Figure 4: The steel structure radial displacements functions (analyzed section).

1, it can be seen that the horizontal displacements are very small, but larger near point No. 11. This can be also observed in the displacement in the radial direction.

Plots presented in Fig. 4 show the diagrams of displacements of points transformed from the components *w* and *u* to the radial direction *r*. The results were obtained from geodetic measurements for the characteristic five stages of backfilling z_g, as presented in Table 1 (marked as A, B, ¼, E). Different backfill levels as presented in Table 1 were used on both sides during the construction process due to the use of twin structures [13]. For this reason, there was an intended lack of symmetry of the structure deformation during backfilling. In the case of the buried steel-soil structure with the largest span in Poland of L=25.724 m built in Ostróda (Poland) (corrugation UltraCor 500 × 237 × 9.65), the deformation symmetry was preserved [11].

4 Estimation of the steel shell radii of curvature

To study the deformation of the steel shell, the change in the radius of curvature at the selected points of the shell [1, 14] is taken into account. Fig. 5 shows a scheme of the location of any of the three chosen (adjacent) points (data obtained from geodetic surveys), highlighting the central point *C*. The coordinates of these points are read by the geodetic measurements and are set in any chosen Cartesian system *G*. The result of the analysis is the determination of the radius of curvature *R* as the distance between the origin of the coordinate system *O* and the measurement points *A*, *C*, *B*. In the case of the section *CO*, this distance which is the radius of curvature can be calculated using the equation

$$R = \sqrt{x_{CO}^2 + z_{CO}^2} \tag{1}$$

Point *O* is determined as a result of parallel transformation from the geodetic coordinate system G(x,z) to computational $O(x_o,z_o)$, defined by the equations

$$x_{OG} = \frac{CA^2 \cdot z_{CB} - CB^2 \cdot z_{CA}}{z_{CA} \cdot x_{CB} - z_{CB} \cdot x_{CA}} \tag{2}$$

and

$$z_{OG} = \frac{CA^2 \cdot x_{CB} - CB^2 \cdot x_{CA}}{z_{CA} \cdot x_{CB} - z_{CB} \cdot x_{CA}} \tag{3}$$

In both equations(2) and (3), there are geometrical relations between the measurement points A,C,B in the geodetic coordinate system G. The distances between the measurement points are

$$CA^2 = CG^2 - AG^2, \tag{4}$$

and

$$CB^2 = CG^2 - BG^2. \tag{5}$$

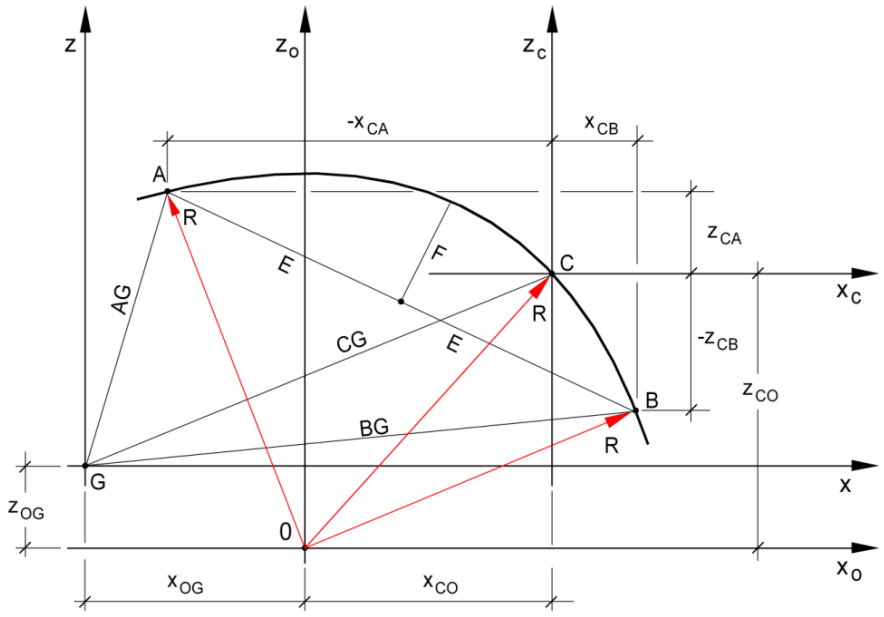

Figure 5: Calculation scheme of the circumferential section of the shell.

The scheme presented in Fig. 5 shows that points A and B are randomly selected in relation to the central point C selected as analyzed. Therefore, in the case of numerous measurement points around the structure periphery, as shown in Fig. 3, any sets of points A and B are possible.

5 Transposing the measurement base to the segment of a circle

By its very nature, measurement points used for geodetic surveys are not regularly arranged on the segment of a circle with a given theoretical radius R, as shown in Fig. 3. The curve formed from these points is not ideally located in the central axis of the steel shell. The distances between the points are not equal, which results from the physical connections of the corrugated plates. Therefore, from the technical point of view, the coordinates of the measurement points do not satisfy the equation of the circle with the designed R value.

After assembly, the steel shell does not, as a rule, form a perfect circular shape. During the backfilling process, when the peaking-up effect is expected for keeping the structure's designed geometry, it is not effective even when the self-weight deflections are relatively easy to determine. This is common due to the quite complex geometry of the steel shell and also the connection slippage. In the construction process, the deformation of the steel structure results from the technology of placement and compacting of the engineering soil material, and hence, the contact interactions between the soil and steel structure are randomized. This is the next reason for the deviations of the measurement line from the theoretical shape.

In this paper, to determine the radius of curvature, the coordinates of the measurement points are used. The circumferential strip line (curve) formed in this way is essential. The inaccuracies of mapping the geometry of the shell based on the *insitu* measurements are corrected as shown in Fig. 6, as in the case of selected point D.

Fig. 6 shows the scheme of the measurement points system, where the deviation value in the radial direction r of this point is calculated from the equation

$$r = \frac{1}{2}\left(\frac{x_{OD}^2 + z_{OD}^2}{R} - R \right). \tag{6}$$

To determine it, equation (1) and the global radius R of the analyzed section of the structure were determined based on coordinates A, B, and C. Assuming different locations of these points, many values of r are obtained. This results, of course, from the fact that the shape of the steel structure defined by the coordinates of the measurement points is not a perfect segment of the circle. If this were the case, we would obtain the same r values regardless of the selection of measuring points.

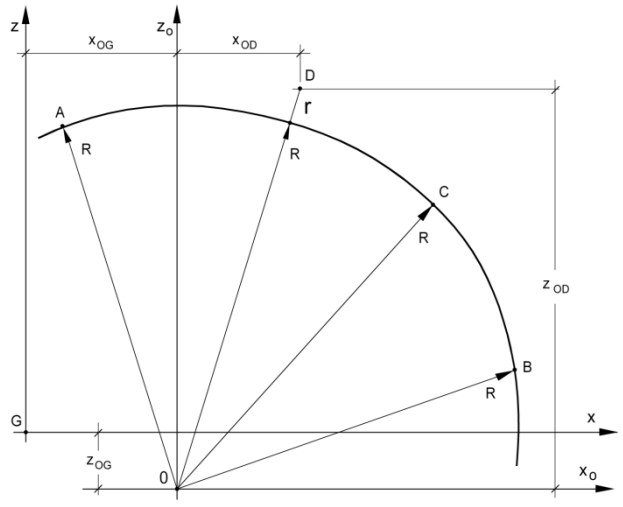

Figure 6: Correction of coordinates of point D.

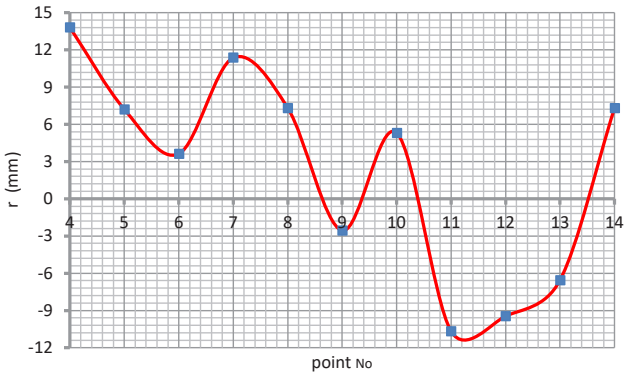

Figure 7: Correction of the location of measurement points around the structure periphery.

Fig. 7 shows the r values treated as a correction of the position of the base of measuring points (reference), when a constant value of R_o=28.443 m was assumed along the entire periphery. The R value was adopted from the analysis of many A C B point sets, following the principle that the r values should be minimal. If only one of the considered sets of points A C B were to be used, the values of r in these points would be zero by default. It can be seen from the graph (see Fig. 7), that the r values are small and also unevenly distributed. However, they significantly affect the R values when points A and B are directly adjacent to point C.

Fig. 5 considers the case of the creation of symmetry from the location of points A and B, when all three points (also C) are located on a circle with radius R. The segment AB (the arc chord) is divided into two equal parts with the values of E. The division point of the arc is spaced with sagitta F. Such a system of points satisfies the equation of an equilateral triangle inscribed in a circle with a given radius R, as in the equation

$$R = \frac{F^2 + E^2}{2F} \,. \tag{7}$$

The methodology of calculating R [1, 11] based on equation (11) does not allow for direct determination of R (F = 0) because when the chord length AB is small, that is, when $F \to 0$ and $E \to 0$ simultaneously, unstable results are obtained. So, it remains to extrapolate the radius of curvature. The accuracy of such estimation is greater when precise geodetic measurements and a dense layout of measurement points are used. It is also necessary to correct the coordinates of the measurement points.

The curve fitting (adjustment to the circular form of an arch) of measurement points should be treated as a computational procedure only. Such a treatment is effective to reduce artificially generated local effects [13]. Coordinates obtained from the geodetic measurements are still important. These points are, by nature, placed randomly, but with the intention of their regular placement. Correction of the coordinates obtained from the geodetic surveys allows for obtaining a uniform R value in the adopted measurement phase (reference).

In practice, it is convenient to use the "z" coordinate correction of the measurement points instead of r, while maintaining the "x" coordinate. For the intermediate point D, it is determined from the equation:

$$\Delta z_D = \frac{1}{2}\left(\frac{R^2 - x_{OD}^2}{z_{OD}} - z_{OD} \right). \tag{8}$$

When analyzing the shell support parts, that is, points 1–4 and 14–17, as shown in Fig.3, and the side parts of closed profiles, it is practical to apply the corrections of the "x" measurement points, as in the equation

$$\Delta x_D = \frac{1}{2}\left(\frac{R^2 - z_{OD}^2}{x_{OD}} - x_{OD} \right). \tag{9}$$

6 Changes of radii of curvature

In practice, there is a global and, therefore, uniform radius of curvature R in the upper part of the structure periphery as shown in Fig.3. The structure is subjected to continuous deformation during construction and service stage, and the structure's shape differs from the perfect

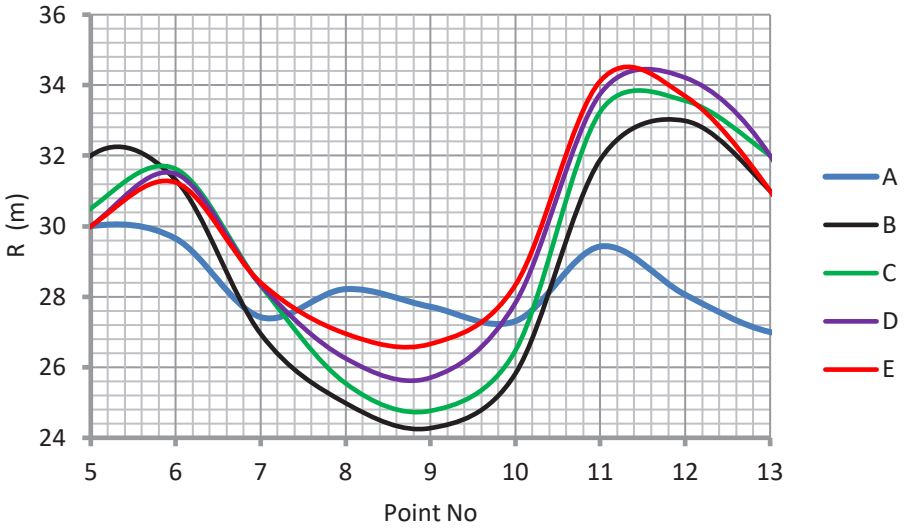

Figure 8: Changes of radii of curvature near the structure crown point.

circular form with some local bulging. Fig. 8 presents the plots of R in analyzed construction stages obtained for the previously mentioned assumptions. The scheme shown in Fig. 5 and equation (1) were used to determine the radius of curvature, and the calculation included a correction of the coordinates of the measurement points as presented in Fig.7.

The R functions presented in Fig. 8 are arranged regularly: minimum values in the structure crown point area and maximum values near the support zone. The values of R are very different in their form, as in the equation for phase B:

$$\frac{R_{\max} - R_{\min}}{R_o} 100\% = \frac{32{,}987 - 24{,}274}{28{,}443} 100\% = 30{,}6\% . \quad (10)$$

The plots of $R$are close to symmetrical with respect to the crown point, as opposed to the r given in Fig. 3. Thus, a static system of the symmetrical single barrel was achieved.

The geometrical parameter used in this study to test the deformation of the steel shell is the change in the curvature κ. The algorithm presented here is based on the results of geodetic measurements. It is obtained based on the radii of curvature: in the analyzed construction stage, R_i refers to the reference value R_o in the selected section as in the equation

$$\kappa(G) = \frac{R_o - R_i}{R_0 \cdot R_i} \quad (11)$$

In the case of structures with record dimensions [Ry, Os], the most common measuring system consists of strain gauges. Therefore, the calculation results obtained from geodetic measurements, as in (9), can be related to the strains [1, 3, 6] included in the equation

$$\kappa(T) = \frac{\varepsilon_g - \varepsilon_D}{f}, \quad (12)$$

when the geometry of the deepest corrugation steel structure is UltraCor a´f´g, while ε_g and ε_D are the strains in the circumferential direction on the upper and lower surfaces of the shell, respectively, accessible from below (air side) [12, 13].

Fig. 9 shows changes in the curvature of the upper part of the circumferential strip of the shell for the construction phase B (when the backfill reaches the level of the structure crown point) and E (in the final stage of the construction of the backfill) as in Table 1. The calculation results obtained from the geodetic measurements (G) were compared to the results of the strain gauge measurements (T).

When assessing the compliance of the results, it should be taken into account that they were obtained from two different measurement techniques. The values of κ(T) are treated as accurate as they were determined at the measuring points. In this case, the plane-remains-plane hypothesis (Euler–Bernoulli) has been taken into account in equation(16). When using geodetic measurements, the curvature is determined based on the location of three points spaced from each other by the value of c. When the geodetic points are significantly distant and there is also

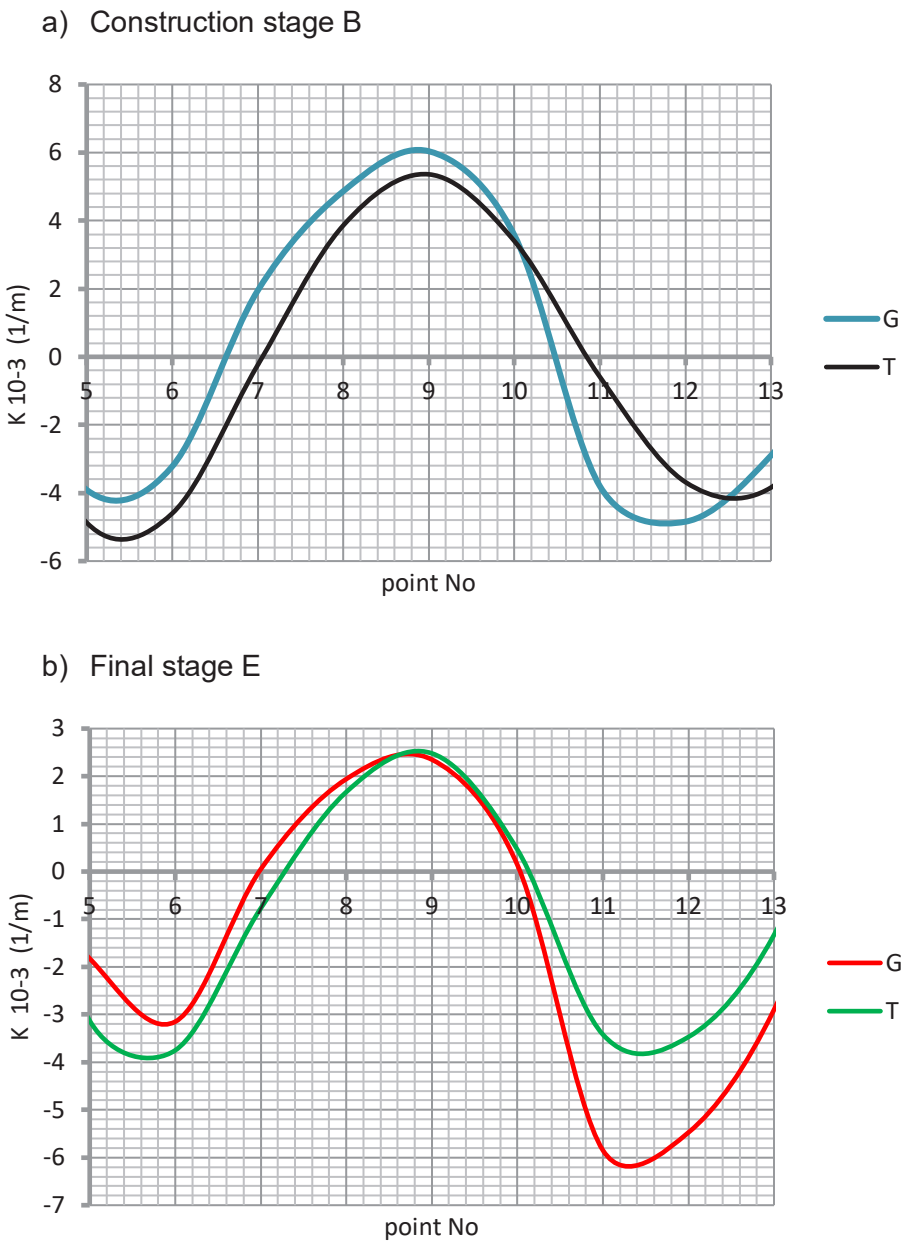

Figure 9: Changes in curvature along the structure periphery.

a significant difference in displacement between them, the accuracy of κ(G) decreases. Therefore, when using geodetic techniques, a dense layout of the measurement points is indispensable.

7 Internal forces due to bending

The algorithm presented in this paper is based on the results of geodetic measurements. The change of curvature is the geometrical parameter used in this study to test shell deformation. Using the strength relation as in the equation

$$M = E \cdot \kappa, \tag{13}$$

it is possible to estimate the bending moments [2, 3, 8] when EI = 22.8 MNm²/m is the bending stiffness of the corrugated steel plate of the analyzed shell. Thus, the results presented in Fig. 9 can be treated as diagrams of bending moments along the periphery of the shell, that is, as a function of s.

The plots in this figure show a large reduction of bending in the area of the structure crown point for the increase in axial forces.

In the case when the backfill has not reached the structure crown point yet, that is, when z_g<H, the aspect of no soil pressure on the crown point can be used, that is, $p = 0$, as in Fig. 2. With this assumption, the relationship of the normal force N with the distribution of bending moments M is as in the equation

$$\frac{N}{R} = \frac{d^2M}{ds^2}, \tag{14}$$

The quantities appearing in (14) are functions, that is, $N(s)$, $M(s)$, and $R(s)$, when s is the distance from the analyzed point but calculated along the circumference of the circular segment of an arch structure. Assuming the differential approach of determining the derivative [7] from (14), the following relation is obtained for the structure crown point:

$$N_9 = \frac{R \cdot EI}{c^2}\left(\kappa_8 - 2\kappa_9 + \kappa_{10}\right), \tag{15}$$

where c = 2.5 m is the distance between the measurement points No.8 and No. 9 and betweenNo.9 and No. 10, as shown in Fig. 3. Taking the data from Fig. 9, for the analyzed construction stage B, it is

$$N_9 = \frac{24{,}274 \cdot 22{,}8 \cdot 10^3}{2{,}5^2} 10^{-3}\left(4{,}865 - 2 \cdot 6{,}038 + 3{,}574\right) = -322{,}1 \ \ kN/m, \tag{16}$$

The value of the normal stress σ on the extreme fibers of the corrugated steel plate, resulting from the bending moment M, can be calculated from (13), taking into account the section modulus W, as in the equation

$$\sigma = \frac{M}{W} = E\frac{f+t}{2}\kappa, \tag{17}$$

The constant factor in equation(17) is a characteristic value of corrugationUltraCor500´237´12and its value is

$$E\frac{f+t}{2} = 205000\frac{0{,}237 + 0{,}012}{2} = 25{,}52 \ \ MN/m, \tag{18}$$

Fig. 9 shows that in phase B, the change of curvature in the crown point is 6.192•× 10^{-3} 1/m. Hence, from (17), the normal stress at the extreme fibers of the corrugated plate is obtained with the value

$$\sigma = 25{,}52 \cdot 6{,}038 = 154 \ \ MPa, \tag{19}$$

The value of normal stress resulting from the axial force calculated in accordance to (16) is

$$\sigma(N) = \frac{N}{A} = \frac{322{,}1 \cdot 10^{-3}}{18{,}04 \cdot 10^{-3}} = 17{,}9 \ \ MPa, \tag{20}$$

The share of the compression in normal stresses is much smaller than the bending effect. Therefore, in the initial stage of construction, it is important to observe the change in the radius of curvature, as shown in Fig. 8. Due to the high values of displacements, as shown in Fig. 3, geodetic measurements are effective for this purpose. In subsequent phases of the backfill placement, the bending effect is significantly reduced, as can be seen in Fig. 9b (phase E).

In the case of determining the soil effects on the steel shell $p(s)$, as in Fig. 2, the equation used is

$$p = \frac{N}{R} + \frac{d^2M}{ds^2}. \tag{21}$$

There are three functions in this equation: $N(s)$, $R(s)$, and $M(s)$. The change in $R(s)$ is essential because, as shown in Fig. 8, it is subject to significant changes. Of course, in the general case, the function $N(s)$ cannot be determined based on the geodetic measurements. Its value can only be estimated, as in equation(15), when z_g<H. The function $p(s)$ can be conveniently determined from strain gauge measurements and strains [8, 9]. Then, the axial force is determined from the equation

$$N = \frac{EA}{2f}\left[(f+t)\varepsilon_g + (f-t)\varepsilon_D\right], \tag{22}$$

and bending moment is determined as

$$M = \frac{EI}{f}\left(\varepsilon_g - \varepsilon_D\right). \tag{23}$$

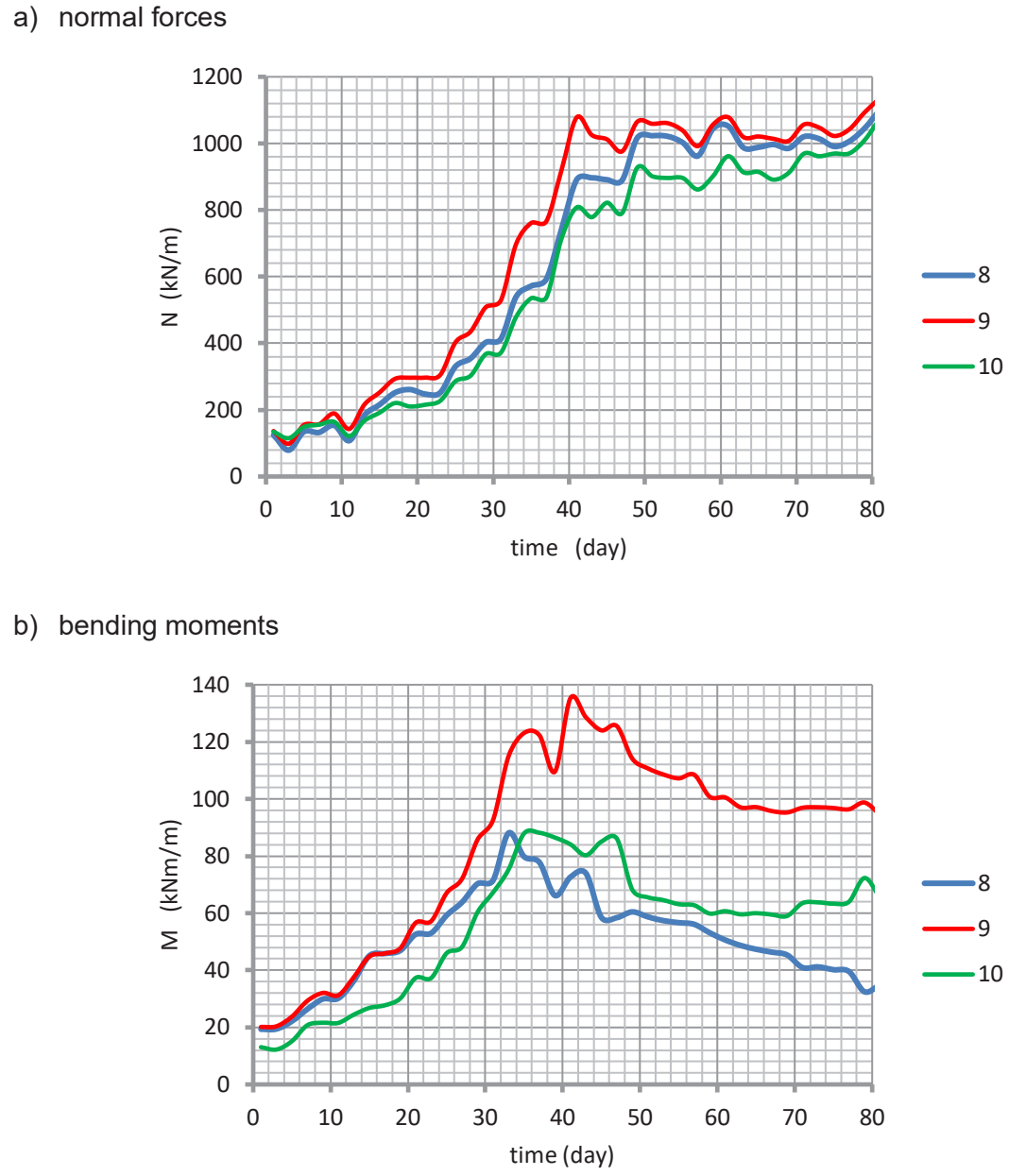

Figure 10: Changes in internal forces in the area of the structure crown point, obtained from strain gauge measurements.

Fig. 10 shows the changes in internal forces in the analyzed period of time between the construction stages A–C. The horizontal axis represents the time (days), where stage A (time = 0). Hence, 37 days are obtained for stage B and 72 days for stage C. The graphs show a very large increase in the axial force between stages A and B, that is, when the backfill is placed in the area of the structure crown point. In the time interval between stages B and C, the increase of N disappears and at the same time the bending moments are reduced. In the figure legend, the numbers of the analyzed measurement points from Fig. 3 are presented.

The graphs in Fig. 10 are used to determine the soil pressure on the shell crown point using equation (21) and the differential approach to the derivative of bending moments, as in equation(15). Fig. 11 shows the change of p in the analyzed period of time between the construction stages A–C. The graph shows the effect of placing the soil layers (backfill and overfill). The arching effect is also observed, consisting of slight changes in soil pressure and

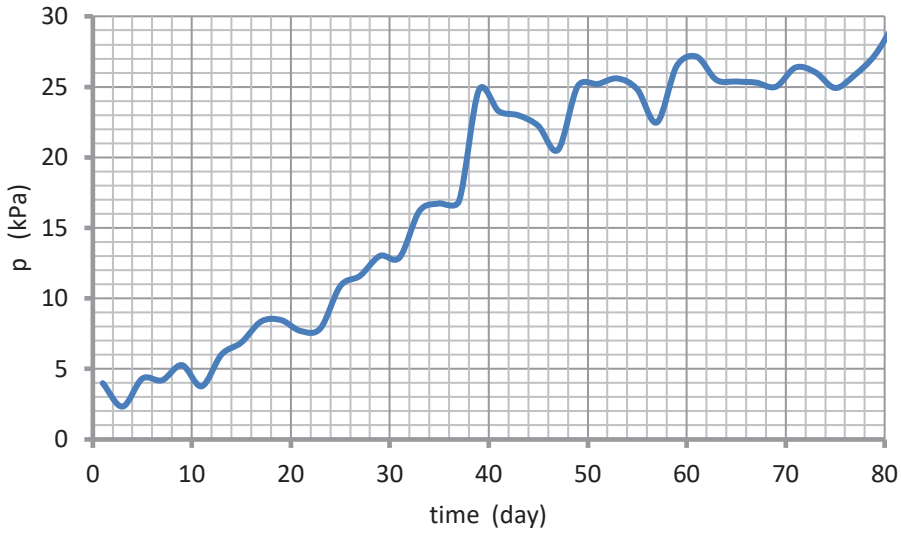

Figure 11: Changes in soil pressure in the structure crown point.

the axial forces with the formation of successive layers of the backfill.

Analysis of Fig. 10a shows a much higher value of N calculated according to equation (16) in stage B. From Fig. 11, It can be seen that the condition $p = 0$ in stage B, which is the base of equation (14). The values of p depend significantly on N and vice versa.

By comparing equations (11) and (12), $R(s)$ is determined from the relationship

$$R(s) = \frac{R_o}{1 + R_o \cdot \kappa(T)}, \tag{24}$$

where R_o is the reference (base) radius and $\kappa(T)$ is the change in the radius of curvature, determined according to (12). Using equation (24), it is possible to determine changes in the radii of curvature as presented in Fig. 8 (in this case, based on geodetic measurements). Using the collocation approach to geometrical relationships presented in [6], based on $R(s)$, the displacements r (s) are determined, as presented in Fig. 4 (resulting from changes in the coordinates of the measurement points). Thus, the results obtained from both measurement techniques, geodetic and strain gauge, can be compared with each other. In assessing the accuracy, however, it should be pointed out that the values at a point are determined by strain gauge measurements and the values for the geodesy are determined along the length of the analyzed peripheral section (in a differential approach).

8 Summary

Usually, deformation and stresses in the shell, created during construction, are many times larger than that occurred during ordinary service of the bridge structure[1, 2, 8]. For this reason, much attention is paid to the construction stage. In the case of extraordinary structures (in a term of span), monitoring is used during backfilling [1, 4, 14, 15, 22]. This paper considers the case of using a dense mesh of measurement points, located around the structure periphery, as the base for geodetic measurements. Changes in the coordinates of these points are used to plot the deformation curve of the shell. This provides data for the calculation of bending moments in the upper part of the shell.

In the algorithm presented in this paper, the results of coordinate measurements are corrected in a way, to adjust them to perfect circular curvature as a reference measurement base during the structure assembly phase. In this way, the inherently irregularly spaced measuring points form a line of points perfectly positioned in the central axis of the corrugated steel structure. The algorithm can also be used for the monitoring of concrete buried structures [22]. In general, this applies not only to ecological structures, but also to road and railway structures where the loads are much higher. In these cases, the long-term effects of the infrastructure facility subjected to multiple variable loads are analyzed.

References

[1] Machelski C.: Badanie konstrukcji gruntowo-powłokowych. Dolnośląskie Wydawnictwo Edukacyjne, Wrocław 2020.

[2] McVay M., Papadopoulos P.: Long term behavior of buried large-span culverts, Journal of Geotechnical Engineering, 112 (4) (1986) 424-442,

[3] MachelskiC.: Soil-steel structure shell displacement functions based on tensometric measurements. Studia Geotechnica et Mechanica 2/2018 p. 55-57 .

[4] Machelski C., Michalski J.B., Janusz L.: Deformation Factors of Buried Corrugated Structures. Journal of the Transportation Research Board. Solid Mechanics. Transportation Research Board of Nationals Academies, Washington D.C. 8/2009 pp. 70-75.

[5] Maleska T. and Beben D. (2019*)* Numerical analysis of soil-steel bridge during backfilling using various shell models. Journal Engineering Structures 196 (1) 1-12.

[6] Miśkiewicz, M.; Sobczyk, B.; Tysiac, P. Non-Destructive Testing of the Longest Span Soil-Steel Bridge in Europe—Field Measurements and FEM Calculations. Materials 2020, 13, 3652. DOI: 10.3390/ma13163652

[7] Beben D.: Application of the interferometric radar for dynamic tests of corrugated steel plate (CSP) culvert. NDT & E International, Elsevier, vol.44, 2011, no. 5, pp. 405–412. Doi: 10.1016/j.ndteint.2011.04.001

[8] MachelskiC.: The use of the collocation algorithm for estimating the deformation of soil-shell objects made of corrugated sheets. Studia Geotechnica et Mechanica 06/2020, 42 (4) p. 319-329.

[9] MachelskiC.: Effects of surrounding earth on shell during construction of flexible bridge structure. Studia Geotechnica et Mechanica 41 (2019) No 2 p. 67-73.

[10] Ahmed M.R., Tran V.D.H., Meguid M.A. : On the role of geogrid reinforcement in reducing earth pressure on buried pipes: experimental and numerical investigations, Soils and Foundations, 55 (3) (2015) 588–599.

[11] Yu W.S., Li Z.L., Xie X.R., Guo L.Y. : Experimental study on earth pressure of corrugated steel culvert under high fill embankment, Applied Mechanics and Materials, 405-408 (2013) 1815-1819,

[12] VaslestadJ.: Soil structure interaction of buried culverts, Institutt for Geoteknikk, Norges Tekniske Hogskole, Universitetet I Trondheim,1990.

[13] Kunecki B.: (2014*)* Field test and tree-dimensional numerical analysis of soil-steel tunnel during backfilling. Journal of the Transportation Research Board. Solid Mechanic, 2462.

[14] Machelski C.: Zmiany promienia krzywizny powłoki mostowego obiektu gruntowo-powłokowego podczas budowy.Changes of radius of curvature of a soil-shell bridge during construction. Drogi i Mosty. Road and Bridges Nr 4/2010 s. 53-72.

[15] Korusiewicz L.: Weryfikacja metody szacowania momentów zginających w obiektach gruntowo-powłokowych na podstawie deformacji powłoki. Verification of the method of estimating bending moments in soil-shell structures on the basis of shell deformation. Drogi i Mosty. Road and Bridges 15 (2016) p. 221-230.

[16] Pettersson L. Flaner E.B, and Sundquist H.: (2015) Design of soil-steel composite bridges. Structural Engineering International 25 (2) 159-192.

[17] Sobótka, M., Łydżba, D. (2019*).* Live load effect in soil-steel flexible culvert: role of apparent cohesion of backfill. European Journal of Environmental and Civil Engineering, 1-15.

[18] Wadi A., Pettersson L., Karoumi R.: Flexible culverts in sloping terrain. Numerical simulation of avalanch load effects. Enginering Structure 2015 ;101 ;111-24

[19] Beben D. and Wrzeciono M.: (2017) Numerical analysis of soil-steel composite (SSC) culvert under static loads. Steel and Composite Structures 23 (6) 715-726.

[20] Bęben D.: Experimental study on the dynamic impacts of service train loads on corrugated steel plate culvert. Journal of Bridge Engineering *ASCE*, 18(4), (2014), 339-346.

[21] Milewski S.: Meshless Finite Difference Method with Higher Order Approximatio-Applications in Mechanics. Arch. Comput. Methods Eng. (2012) 19 :1-49

[22] Jenkins D.A.: Non-Linear Analysis of Buried Arch Structures. Australian Structural Engineering Conference, Auckland 30-2 October 1998.

[23] Wadi, A. (2015). Flexible culverts in sloping terrain: Research advances and application. (Licentiate dissertation). Stockholm: KTH Royal Institute of Technology